A Novel Computational Model of the Zebrafish Atrial Action Potential and Intracellular Calcium Transient

Zachary D Long[1], Ludovica Cestariolo[2], Jose Maria Ferrero[3],
T Alexander Quinn[1], Jose F Rodriguez Matas[2]

[1]Dalhousie University, Halifax, Canada
[2]Politecnico di Milano, Milan, Italy
[3]Universitat Politecnica de Valencia, Valencia, Spain

Abstract

The zebrafish has emerged as a valuable experimental model for studying cardiac electrophysiology and arrhythmias, yet there are no detailed computational models specific to its atrial action potential (AP) and intracellular calcium (Ca^{2+}) transient (CaT). We present a novel zebrafish-specific model, integrating experimental data from microelectrode and optical mapping recordings in the adult heart. We used a combination of experimental measurements and simulations to calibrate the model and validate it against additional experimental data. The model successfully reproduces experimentally observed atrial AP and CaT under various physiological conditions, offering a valuable tool for future work involving disease modelling, drug screening, and the investigation of cardiac arrhythmias.

1. Introduction

The zebrafish (*Danio rerio*) is an increasingly important experimental model for a broad range of applications due to its strikingly similar cardiac and neuronal genetics [1] and function [2,3] compared to human. This allows the zebrafish to be used for a wide range of research applications, including developmental, pharmacological, oncological, neuronal, and cardiovascular. Regarding the heart, the zebrafish AP closely resembles that of humans in both shape and duration, primarily due to comparable ion channel composition and properties [2]. This makes zebrafish an attractive model for studying cardiac (patho-)physiology and pharmacology [4].

While many species-specific computational AP models exist, and in combination with experimental studies have been instrumental in gaining fundamental insight into cardiac (patho-)physiology, there are currently no zebrafish-specific models for the atria. Our group has recently developed a computational AP model for the zebrafish ventricle [5]; here we present the development of an accompanying atrial model.

2. Methods

2.1. Experimental preparation

All experimental procedures were approved by the Dalhousie University Committee for Laboratory Animals, following previously published protocols [6]. Adult wild-type AB zebrafish (11-13 months post-fertilisation) from a mixed sex population were utilised. Zebrafish were anaesthetised with 1.5 mM tricaine in Tris-buffered (pH 7.4) 28°C tank water until opercular movement stopped. A ventral midline incision was made through the body wall and a block of tissue encompassing the ventral aorta, ventricle, atrium, and sinus venosus was removed. The heart was maintained in 28°C HEPES-buffered saline solution (in mM: 135 NaCl, 5 KCl, 5.5 $NaHCO_3$, 1.5 NaH_2PO_4, 1.7 $MgCl_2$, 1.8 $CaCl_2$, 7.5 Glucose, 5 Creatine, 10 HEPES). An atrial surface electrocardiogram (ECG) was collected with a custom suction microelectrode connected to an ECG amplifier. The atrium was paced at 2 Hz to control for heart rate (HR).

2.2. Pacing protocol

Steady-state pacing, S1-S2, and dynamic restitution protocols were performed. For the steady-state pacing protocol, 300 stimuli were delivered to the heart, with cycle lengths of 1000, 500, or 200 ms. For the S1-S2 restitution protocol, after 10 stimuli at a cycle length of 500 ms (S1), a single premature stimulus of a shorter cycle length (S2) was delivered. The S1-S2 coupling interval was progressively shortened from 500 to 100 ms, with a varying step size. For the dynamic restitution protocol, trains of 100 stimuli were delivered to the heart, with a decreasing cycle length for each stimulus train.

 ISSN: 2325-887X DOI: 10.22489/CinC.2024.330

2.3. AP measurements

Intracellular microelectrode recordings of membrane potential (V_m) were performed as previously described [6]. The measured V_m was taken as the difference between the potential inside the microelectrode and a silver-chloride wire in the bath. The tip of the electrode was moved *via* a mechanical manipulator into the mid-atrial epicardium until an AP signal was obtained. Criteria for a successful cell impalement and data inclusion were an AP with a stable resting membrane potential (RMP) <-60 mV and peak V_m >0 mV maintained throughout the recording.

2.4. Intracellular Ca^{2+} measurements

Hearts were incubated with 0.02% pluronic acid in saline solution for 1 min. 5 µM Fluo-5F AM was added to the bath along with 10 µM of the excitation-contraction uncoupler ±blebbistatin to minimize artifacts associated with movement during contraction. Hearts were incubated in Fluo-5F for 20 min and replaced with a saline solution containing 10 µM ±blebbistatin and 1 mM probenecid and left for 30 min to allow for dye de-esterification and cessation of contraction. Hearts were epi-illuminated with a mercury arc lamp through an upright microscope with a 5× objective. Fluo-5F was excited for 5 s periods with light passing through a 466±20 nm filter and reflected by a 495 nm dichroic mirror. Emitted fluorescence was passed through a 574±69 nm filter and captured with an EMCCD camera at 500 frames/s.

2.5. Data analysis

The last 10 AP or CaT for each cycle length in the steady-state or dynamic pacing protocols, or the S2 beat of the S1-S2 protocol, were analysed. For AP analyses, RMP (stable V_m during diastole), maximum AP upstroke speed (dV_m/dt_{max}), AP amplitude (APA, difference between peak V_m and RMP), and action potential duration (APD_X, time from the point of dV_m/dt_{max} to X% V_m repolarisation) were calculated and averaged. For CaT analysis, CaT upstroke speed (dF/dt_{max}) and CaT duration ($CaTD_X$, time from the point of dF/dt_{max} to X% decline in fluorescence from peak).

2.6. Numerical formulation

The atrial model was adapted from our zebrafish-specific ventricular AP model, which was based on the Ten Tusscher and Panfilov (TP04) formulation (Fig. 1) [5,7]. In contrast to human, the zebrafish atria do not express the transient potassium current (I_{to}), so it was removed, while the T-type Ca^{2+} current (I_{CaT}) was added using a formulation from models of the rabbit sinoatrial node [8,9].

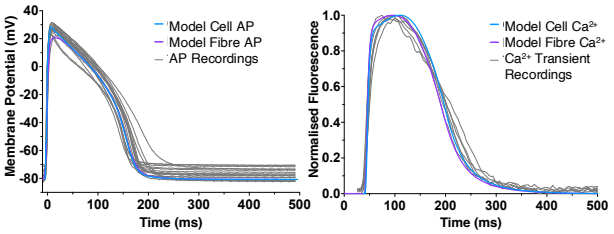

Figure 1. Comparison of experimental and computational AP and CaT with a BCL of 500 ms.

The final atrial model included the following currents: fast sodium (I_{Na}); I_{CaT}; L-type Ca^{2+} (I_{CaL}); rapid and slow delayed rectifier potassium (I_{Kr}, I_{Ks}); inward rectifier potassium (I_{K1}); sodium-Ca^{2+} exchanger (I_{NaCa}); sodium-potassium pump (I_{NaK}); Ca^{2+} pump (I_{pCa}); and background sodium (I_{bNa}) and Ca^{2+} (I_{bCa}).

The equation describing V_m can be expressed as:

$$C_m \frac{dV_m}{dt} = I_{ion} - I_{stim} \quad (1)$$

where C_m is cell membrane capacitance, t is time, I_{stim} is the externally applied stimulation current, and I_{ion} is the sum of the ionic currents:

$$I_{ions} = I_{Na} + I_{CaT} + I_{CaL} + I_{Ks} + I_{Kr} + I_{K1} + I_{NaCa} + I_{NaK} + I_{pCa} + I_{bNa} + I_{bCa} \quad (2)$$

A 1-dimensional fibre of atrial myocytes was modelled as a continuum, with the following equation:

$$C_m \frac{\partial V_m}{\partial t} = \sigma \frac{\partial^2 V_m}{\partial^2 t} - I_{ion} - I_{stim} \quad (3)$$

where σ is the fibre conductance. Numerical integration was performed using the forward Euler method with a space discretization of Δx=0.01 mm and a time step of Δt=0.02 ms. A conductance of σ=0.301 μS produced a conduction velocity of 16.05 mm/s, in agreement with our optical mapping experiments. To integrate the Hodgkin-Huxley equations for the various time-dependent channel gating variables, the Rush-Larsen scheme was used.

2.7. Model calibration and validation

The gating variables of ionic currents were re-parameterised using zebrafish patch clamp data from the literature [10-14]. Ion channel conductances were then calibrated by fitting the model with single cell and fibre simulations to the experimental AP and Ca^{2+} transient recordings during steady-state pacing at the various cycle lengths using a Monte-Carlo and sensitivity analysis approach, involving variations of maximum current conductance (and other select variables) by ±15% and shifting activation or inactivation curves by ±5 mV. Cell and fibre simulations were then run to validate the model against the experimental restitution data.

3. Results

The developed model exhibited stable AP and CaT. Fig. 2 shows the AP and CaT generated with cell and fibre simulations, compared to experimental recordings. Table 1 shows the associated AP and CaT parameters measured from the fibre simulations, which fit well within the experimentally recorded ranges (Table 1).

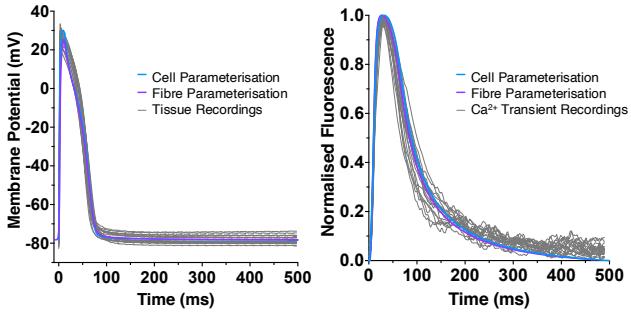

Figure 2. Comparison of experimental and computational AP and CaT with a BCL of 500 ms.

Table 1: Experimental (mean±SD) and computational parameters for the fibre simulations with a BCL of 500 ms.

Parameter	Model	Experiment (n=18)
APD_{80} (ms)	66	64±4
APD_{50} (ms)	52	52±4
dV_m/dt_{max} (mV/ms)	39	36±4
RMP (mV)	-78	-79±3
APA (mV)	103	104±4
dF/dt_{max} (ms^{-1})	0.009	0.002±0.001
$CaTD_{80}$ (ms)	145	141±22
$CaTD_{50}$ (ms)	78	75±9

The APD_{80} (Fig. 3) and $CaTD_{80}$ (Fig. 4) S1-S2 restitution curves (as well as the dynamic restitution curves, not shown) for the cell and fibre simulations fell within the experimentally measured ranges. The restitution curves for dV_m/dt_{max}, RMP, APA, and dF/dt_{max} were also in line with experimental data (not shown), with a few exceptions. dV_m/dt_{max} of AP for cell simulations was higher than experimental values at slow HR, but was corrected in fibre simulations, presumably due to electrotonic coupling with neighbouring cells. RMP on the other hand fit well at slower HR but lacked the upward deflection at higher HR. While APA for both cell and fibre simulations fit the experimental curves, APA was lower in fibre simulations, again presumably due to electrotonic coupling. For CaT, dF/dt_{max} fell outside of experimental values at some HR and also differed between cell and fibre simulations.

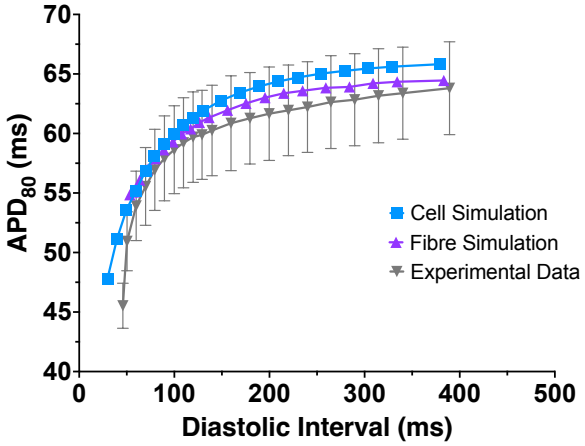

Figure 3. Experimental and computational fibre simulation S1-S2 APD_{80} restitution curves.

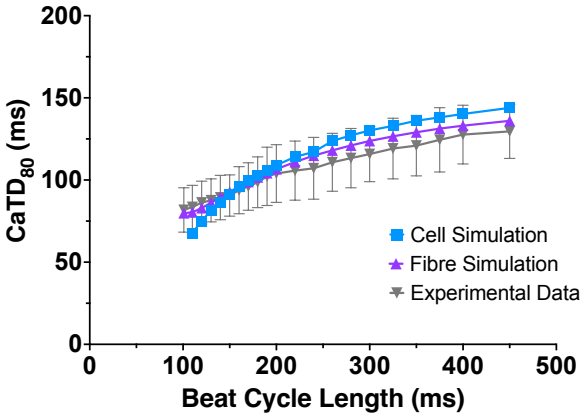

Figure 4. Experimental and computational fibre simulation S1-S2 $CaTD_{80}$ restitution curves.

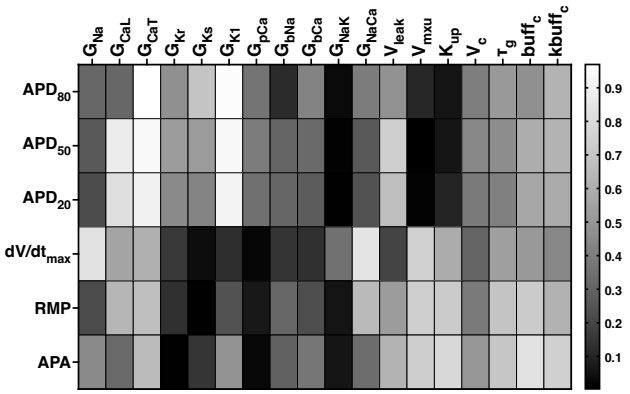

Figure 5. Heat map of the sensitivity analysis for fibre simulations showing the influence of the principal current conductances on measured AP parameters.

Fig. 5 shows a heat map of the sensitivity analysis for fibre simulations showing the influence of the principal current conductances on the AP parameters listed in Table 1. Results indicate that APD is particularly sensitive to the conductance of currents involved in the AP plateau and repolarisation (*i.e.*, G_{CaL}, G_{CaT}, and G_{K1}) and the sodium-potassium pump (G_{NaK}), as well as Ca^{2+} reuptake dynamics (V_{mxu} and K_{up}).

4. Discussion

This work presents the development and validation of the first computational model of the zebrafish atrial AP and CaT, parameterised and validated using novel experimental data from the adult heart.

Single cell and fibre simulations performed with the model closely replicate zebrafish AP and CaT morphology (Fig. 2), with most of the measured parameters of interest within experimental ranges (Table 1). Cell and fibre simulations of restitution experiments also generally fit the experimental curves (Figs. 3 and 4). Cases where differences from experimental behaviour exist may be driven by the lack of zebrafish-specific data for some ion channels in the atria, highlighting the need for further patch clamp experiments and model refinement. Further model development may be guided by the results of the accompanying sensitivity analysis, which provides insight into parameters with the greatest influence on specific AP parameters (Fig. 5).

5. Conclusion

We have developed the first zebrafish-specific computational model of the atrial AP and CaT. The cell and fibre simulations performed with the model generate AP and CaT morphologies seen experimentally, with transient parameters that fit within experimental ranges. Further work is needed to improve rate-dependent behaviour of the model, as new patch clamp data becomes available. Overall, the new model represents a useful novel tool for (patho)physiological experimental-computational studies of cardiac electrophysiology involving zebrafish.

Acknowledgments

We would like to acknowledge the staff of the Dalhousie Zebrafish CORE Facility for their assistance with this study.

References

[1] K. Howe et al., "The zebrafish reference genome sequence and its relationship to the human genome," *Nature*, vol. 496, no. 7446, pp. 498–503, Apr. 2013.

[2] U. Ravens, "Ionic basis of cardiac electrophysiology in zebrafish compared to human hearts," *Prog. Biophys. Mol. Biol.*, vol. 138, pp. 38–44, Oct. 2018.

[3] M. R. Stoyek, L. Hotells, and T. A. Quinn. "From mice to mainframes: experimental models for investigations of the intracardiac nervous system," *J. Cardiovasc. Dev. Dis.*, vol. 8, no. 11, Nov. 2021, Art. No. 149.

[4] M. R. Stoyek, and T. A. Quinn. "One fish, two fish, red fish, blue fish: zebrafish as a model for cardiac research," *Prog. Biophys. Mol. Biol.*, vol 138, pp. 1–2, Oct. 2018.

[5] L. Cestariolo, J. M. Ferrero, Z. Long, T. A. Quinn, and J. F. R. Matas, "Towards the development of an *in silico* model for the zebrafish action potential," *Comput. Cardiol.*, vol. 50, Oct. 2023.

[6] M.R. Stoyek et al., "*POPDC1* variants cause atrioventricular node dysfunction and arrhythmogenic changes in cardiac electrophysiology and intracellular calcium handling in zebrafish," Genes., vol. 15, Feb. 2024, Art. No. 280.

[7] K. H. W. J. Ten Tusscher, D. Noble, P. J. Noble, and A. V. Panfilov, "A model for human ventricular tissue," *Am. J. Physiol. Heart Circ. Physiol.*, vol. 286, no. 4, pp. H1573–H1589, Apr. 2004.

[8] S. S. Demir, J. W. Clark, C. R. Murphey, and W. R. Giles, "A mathematical model of a rabbit sinoatrial node cell," *Am. J. Physiol.*, vol. 266, pp. C832-C852, Mar. 1994.

[9] H. Zhang *et al*., "Mathematical models of action potentials in the periphery and center of the rabbit sinoatrial node," *Am. J. Physiol. Heart Circ. Physiol.*, vol. 279, no. 1, pp. H397–H421, Jul. 2000.

[10] S. S. Chopra, H. Watanabe, T. P. Zhong, and D. M. Roden, "Molecular cloning and analysis of zebrafish voltage-gated sodium channel beta subunit genes: implications for the evolution of electrical signaling in vertebrates," *BMC Evol. Biol.*, vol. 7, Jul. 2007, Art. No. 113.

[11] J. Haverinen, M. Hassinen, S. N. Dash, and M. Vornanen, "Expression of calcium channel transcripts in the zebrafish heart: dominance of T-type channels," *J. Exp. Biol.*, vol. 221, May 2018, Art. no. jeb179226.

[12] P. C. Zhang, A. Llach, X. Y. Sheng, L. Hove-Madsen, and G. F. Tibbits, "Calcium handling in zebrafish ventricular myocytes," *Am. J. Physiol. Regul. Integr. Comp. Physiol.*, vol. 300, no. 1, pp. R56–R66, Jan. 2011.

[13] D. V. Abramochkin, M. Hassinen, and M. Vornanen, "Transcripts of K_V7.1 and MinK channels and slow delayed rectifier K^+ current (I_{Ks}) are expressed in zebrafish (*Danio rerio*) heart," *Pflugers Arch.*, vol. 470, no. 12, pp. 1753–1764, Dec. 2018.

[14] E. P. Scholz et al., "Biophysical properties of zebrafish ether-à-go-go related gene potassium channels," *Biochem. Biophys. Res. Commun.*, vol. 381, no. 2, pp. 159–164, Apr. 2009.

Address for correspondence:

Zachary Long
Cardiac Autoregulation and Arrhythmias Laboratory, 4J
Dept. of Physiology and Biophysics, Dalhousie University
5850 College Street, Halifax, NS, B3h 4R2, Canada
zlong@dal.ca